Bioactive Materials 6 (2021) 749–756

Contents lists available at ScienceDirect

Bioactive Materials

journal homepage: http://www.keaipublishing.com/biomat

Conferring receptors on recipient cells with extracellular vesicles for targeted drug delivery

Zachary Quinn[a,1], Wenjun Mao[b,**,1], Yiqiu Xia[c], Rhea John[a], Yuan Wan[a,*]

[a] The Pq Laboratory of Micro/Nano BiomeDx, Department of Biomedical Engineering, Binghamton University-SUNY, Binghamton, NY, 13902, United States
[b] Department of Cardiothoracic Surgery, The Affiliated Wuxi People's Hospital of Nanjing Medical University, Wuxi, Jiangsu, 214023, PR China
[c] Department of Biomedical Engineering, Carnegie Mellon University, Pittsburgh, PA, 15213, United States

ARTICLE INFO

Keywords:
Extracellular vesicles
Drug delivery
Triple-negative breast cancer
HER2

ABSTRACT

Triple negative breast cancer (TNBC) is a heterogeneous subset of breast cancer characterized by its lack of estrogen receptor, progesterone receptor, and human epidermal growth factor receptor 2 (HER2), which altogether prevents TNBC from being treated effectively. For many years, the treatment paradigms and overall survival of patients with TNBC have remained largely stagnant. Recent attempts to convert cold tumors to hot tumors by promoting antigen presentation have shown increased T cell infiltration and significantly induced immune responses for tumor killing. Inspired by this concept, the expression of specific targetable antigens on TNBC cells may further benefit relevant targeted drug delivery. In this study, we successfully conferred sufficient HER2 on the surface of TNBC MDA-MB-231 cells via simple EV-plasma membrane fusion with HER2+ extracellular vesicles (EV) derived from HER2 overexpressing BT-474 cells. Subsequently, anti-HER2 antibody conjugated paclitaxel-loaded liposomes were used for HER2-targeted drug delivery. Our findings demonstrated this HER2 grafting, in conjunction with targeted drug delivery, can improve the treatment efficacy *in vitro* and *in vivo*. This novel approach represents a facile method of altering cell membrane antigen presentation via convenient EVs uptake and may pave the way for the burgeoning wave of targeted therapy and/or immunotherapy.

1. Introduction

Triple negative breast cancer (TNBC) is a heterogeneous subset of breast cancer (BC) characterized by a lack of estrogen receptor, progesterone receptor, and human epidermal growth factor receptor 2 (HER2) [1,2]. Accounting for 15–20% of total instances of BC, TNBC is most prevalent in the African American and Hispanic community, as well as in younger women [3]. Compared to other BCs, TNBC is very aggressive, more likely to metastasize within 5 years of diagnosis, and yields poorer prognoses than other subtypes [4–7]. Overall, TNBC patients generally exhibit shorter median times to death and poorer overall survivals (OS) [5,8,9]. While TNBC appears to be more receptive to neoadjuvant chemotherapy than other receptor positive subtypes, it is definitively less susceptible to receptor-based targeted drug delivery or immunotherapy [8,10]. Hence, over the past few decades, treatment paradigms and OS have remained relatively stagnant.

Immune checkpoint therapy using monoclonal antibodies has all but revolutionized the treatment of many cancers, such as non-small cell lung cancer, melanoma, and renal cell carcinoma [11–13]. Specifically in BC, immunotherapeutic and hormone receptor treatments such as trastuzumab have significantly improved the OS of patients with tumors expressing these targetable receptors [14]. Of note, this benefit is not universal. Many cancers, even typically susceptible subsets, often show limited responses while other forms are resistant to immunotherapy entirely [11]. Moreover, the development of adaptive resistance to immunotherapies is extremely common. To this end, significant research has been dedicated to the conversion of 'cold' tumors, wherein scarce adaptive or innate immune response has taken place, to 'hot' or inflamed tumors [15,16]. The latter typically represent a population more conducive to immunotherapeutic agents. In an effort to heat cold tumors up, various techniques have been used including priming T cell activation via targeted radiotherapy, oncolytic viral therapies, or the use of immunocytokines to promote T cell infiltration [16]. In brief, a

Peer review under responsibility of KeAi Communications Co., Ltd.
* Corresponding author. Biotechnology Building, Room 2625, 65 Murray Hill Road, Vestal, NY, 13850, United States.
** Corresponding author. Qingyang Road, Wuxi, Jiangsu, 214023, PR China.
E-mail addresses: maowenjun1@njmu.edu.cn (W. Mao), ywan@binghamton.edu (Y. Wan).
[1] Equal Contribution.

https://doi.org/10.1016/j.bioactmat.2020.09.016
Received 30 July 2020; Received in revised form 23 August 2020; Accepted 15 September 2020

major key for transforming cold tumors to hot is the alteration of specific antigen presentation on cancer cells to encourage immune cell-mediated tumor killing. To this end, previous studies have attempted to express specific targetable antigens on TNBC cells for treatment. Demethylating agents and other epigenetic drugs have been successful in modulating cellular antigen presenting machinery, thereby creating specific treatment targets [17,18]. However, these attempts fail to specifically imprint desired receptors on the cell membrane surface.

EVs are lipid-bilayer encapsulated particles released by virtually all eukaryotic cells. As mediators of intercellular communication, EVs are intimately involved with a wide range of pathophysiological mechanisms via transfer of functional protein/RNA contents to nearby or distant recipient cells. In cancer, the role of EVs in the induction of pre-metastatic, metastatic, and pro-tumorigenic activity of both healthy and cancerous cells via EV uptake has been previously substantiated [19–28]. Moreover, the use of EVs in cancer treatment has received considerable attention due in part to their advantages over artificial nanoparticles, including their innate biocompatibility, excellent extravasation, and extended blood circulation half-life [29–33]. Furthermore, EVs can fuse with the cell membrane and deliver drugs directly into the cytoplasm. By evading engulfment by lysosomes, EVs remarkably enhance delivery efficiency of vulnerable molecules [34,35]. Meanwhile, during membrane fusion, EV-harboring membrane antigens will be integrated into the plasma membrane of recipient cells [36,37]. Therefore, EVs have been exploited as drug vehicles for drug delivery. However, to the best of our knowledge EVs have not been explored to alter the phenotype of recipient cells for subsequent therapy. Based on these EV features, it is possible to speculate that EVs released from HER2-overexpressing BT-474 cells can directly impose HER2 on TNBC MDA-MB-231 cells, and thus confer MDA-MB-231 cells with targetable receptors for selective delivery of chemotherapeutic drugs. Here, we report HER2+ EV-educated MDA-MB-231 cells can be efficiently treated with HER2-targeted paclitaxel (PTX) *in vitro* and *in vivo*.

2. Materials and methods

Cell culture. MDA-MB-231 cells were maintained in DMEM supplemented with 5% FBS. BT-474 cells were cultured in McCoy's 5a medium containing 5% FBS. All cells passed testing for mycoplasma contamination. Cells were cultured in a humidified atmosphere of 5% CO2 at 37 °C. Alexa Fluor 594 conjugated antibody (Santa Cruz, sc-33684, 1:50) was used to identify HER2 on cell membrane. In brief, BT-474 cells, MDA-MB-231 cells, and BT-474 EVs educated MDA-MB-231 cells were fixed with 4% paraformaldehyde at 4 °C for 30 min followed by PBS rinsing thrice. Without cell membrane permeabilization, DAPI and fluorescence tagged HER2 antibodies were subsequentially incubated with cells at 4 °C for 10 min and 2 h. After PBS washing, cells were observed with a fluorescence microscope (Olympus).

EV harvest. BT-474 cells at 70% confluence were maintained with FBS-free medium for 24 h. The supernatant was collected and centrifuged at 20,000*g* for 15 min to discard cellular debris. Afterward, a total of 120 mL of supernatant was collected and ultracentrifuged at 100,000 *g* continuously at 4 °C for 2 h. EV pellets were suspended in 200 μl of PBS and stored at −80 °C until use. Similarly, MDA-MB-231 EVs were harvested following the exact same protocol.

EV characterization. 10 μl EV samples were loaded on 400-mesh Formvar-coated copper grids and allowed to incubate for 3 min at room temperature (RT). Excess samples were drained with filter paper and stained with 1% filtered uranyl acetate solution for 1 min. Prepared samples were imaged with a Hitachi TEM at an accelerating voltage of 100 kv. Size distribution and concentration of BT-474 EVs were measured with Nanosight NS300 according to manufacturer's instructions followed by automated analysis.

Western blot. After lysis with RIPA buffer, protein amount in cells were determined using Micro BCA Protein Assay (Pierce). Cell membrane protein was extracted with Mem-PER Plus Membrane Protein Extraction Kit (Thermo Fisher, 89,842) following the manufacturer's instruction. Protein samples were analyzed using acrylamide gels, and then transferred onto polyvinylidene difluoride membranes. The protein blot was blocked for 1 h at RT with 5% nonfat dry milk in PBS/0.05% Tween 20 and incubated overnight at 4 °C with antibodies against HER2 (sc-33684, 1:500), β-actin (sc-47778, 1:500), and integrin (sc-9970, 1:500). Afterward, secondary antibodies were incubated for 1 h at RT. Samples were washed with PBS/0.05% Tween 20 for 10 min thrice. Blots were developed with chemiluminescence. Similarly, BT-474 EV protein was characterized, and MDA-MB-231 EV protein was used as a control. Following the protocol described above, antibodies against HER2, CD9 (sc-13118, 1:500), and TSG101 (sc-7964, 1:500) were used to determine the amount of HER2 on EV and the other two canonic EV markers.

Education of MDA-MB-231 cells with BT-474 EVs. To optimize time of cell education with EVs, approximately 4×10^4 MDA-MB-231 cells in 96-well plate were educated with 1×10^{10} BT-474 EVs for 2, 6, and 12 h. After incubation, supernatant was removed, and MDA-MB-231 cells were thoroughly rinsed with PBS thrice to remove surplus unbounded BT-474 EVs. Next, 1×10^7, 1×10^8, 1×10^9, and 1×10^{10} BT-474 EVs were used to educate MDA-MB-231 cells for 12 h followed by thorough rinsing. The amount of HER2 in educated MDA-MB-231 cells and counterparts was determined by Western blot.

Wound-healing assay. 4×10^4 MDA-MB-231 cells were seeded into each well of a 96-well plate and were allowed to attach onto the substrate overnight. When confluence reached 100%, a pipette tip was used to scratch the cell monolayer. Detached cells were removed by replacing the medium. Cells were educated with $\sim 1 \times 10^{10}$ BT-474 EVs for 12 h. The width of the wound was monitored under the microscope at 0, 24, and 48 h time points. ImageJ was used to calculate the wound area.

Liposome preparation and characterization. PTX-loaded liposomes (LP-PTX) were prepared following the widely used protocol [38]. Liposomes were composed of DSPC (Avanti, 850365C), Cholesterol, and DSPE-PEG_{2000}-maleimide (NanoCS, PG2-DSML-2k) at respective molar ratio of 70:25:5. Excess free PTX was removed from LP-PTX with a Sephadex G25 column. Then, the anti-HER2 antibodies (Santa Cruz, sc-33684) were covalently conjugated onto liposomes at a molar ratio of 1:10 for 4 h at 4 °C followed by ultracentrifugation at 180,000 *g* and 4 °C for 1 h to remove unconjugated antibodies. The size distribution and zeta potential of liposome and anti-HER2-liposome (Ab-LP) were routinely measured. The amount of loaded PTX in each group was measured by high-performance liquid chromatography (HPLC). To measure PTX release, freshly prepared LP-PTX and Ab-LP-PTX were placed in a 300 kDa molecular weight cutoff dialysis membrane (Spectrum Labs). The device was then placed in PBS at room temperature with stirring. Samples were taken at time points and analyzed by HPLC. Before treatment of MDA-MB-231 cells with Ab-LP-PTX, we examined whether educated MDA-MB-231 cells harbor HER2 derived from BT-474 EVs. TopFluor Cholesterol (Avanti, 810,255) was used to prepare Ab-LP bearing green fluorescence following the above-mentioned protocol. Approximately 4×10^4 MDA-MB-231 cells in a single well of 96-well plate ($n = 5$) were incubated with 1 pmole Ab-LP at 37 °C for up to 20 min. Fluorescence images were taken every 5 min.

Therapeutic efficacy *in vitro*. The respective IC_{50} values of free PTX, LP-PTX, and Ab-LP-PTX in BT-474 EV-educated MDA-MB-231 cells were determined with an MTT assay (ThermoFisher Scientific) following the manufacturer's instructions. 3×10^5 MDA-MB-231 cells were seeded into each well of a 6-well plate and were allowed to attach onto the substrate overnight. Cells were educated with $\sim 1 \times 10^{11}$ BT-474 EVs for 12 h. Subsequently, MDA-MB-231 cells in 4 groups were, respectively, treated with PBS, 100 nmol/L free PTX, LP-PTX, and Ab-LP-PTX for 24 h. A total of 5×10^5 harvested MDA-MB-231 cells in 100 mL binding buffer (BD Biosciences) were incubated with 10 mL

propidium iodide (PI) and 5 mL of Annexin V-FITC for 30 min at RT. Each sample was analyzed by flow cytometry. With the same experimental setup, cells in 4 groups were stained with PI only and photographed.

Therapeutic efficacy *in vivo*. Approximately 1×10^6 uneducated MDA-MB-231 cells in 50-mL PBS mixed with 50 mL of Matrigel were inoculated subcutaneously to the flanks of 6-week BALB/c mice (n = 4), and allowed to grow to a tumor size approximately 100 mm^3. The mice were then randomly divided into 4 groups. Before drug or PBS infusion, $\sim 3 \times 10^{11}$ BT-474 EVs were directly injected into solid tumors at multiple sites with a 30G needle. After 12 h inoculation, PBS, free PTX or Ab-LP-PTX was then intravenously administered every 2 days (2 mg of PTX-equivalent per kg of body weight per dose) for 3 weeks. Mice were euthanized to harvest tumors. All animal experiments were approved by and performed in accordance with guidelines from the Institutional Animal Care and Use Committee (IACUC) of the Model Animal Research Center of the Wuxi People's Hospital Affiliated to Nanjing Medical University (Wuxi, Jiangsu, China).

Statistics Analysis. Results are presented as mean ± standard deviation (SD). Statistical comparisons were performed by two-tailed T-test and two-tailed ANOVA test. A p-value < 0.05 was considered statistically significantly.

3. Results

Characterization. Previous studies reported that the average amount of HER2 on MDA-MB-231 cells and BT-474 cells is $\sim 4 \times 10^4$ and $\sim 4 \times 10^6$, respectively [39–41]. The fluorescent staining confirmed that HER2 fluorescence signal was either undetectable or extremely weak in MDA-MB-231 cells, demonstrating the former is HER2 low expressing (Fig. 1a). By contrast, BT-474 cells overexpress HER2 [42]. This was further confirmed with Western blot analysis of cell lysates derived from MDA-MB-231 cells and BT-474 cells (Fig. 1b). In addition, Western blot analysis also confirmed the dearth of HER2 in lysates of MDA-MB-231 EVs and its presence within BT-474 EV lysates (Fig. 1c). Meanwhile, EV canonic protein markers CD9 and TSG-101 were identified in both MDA-MB-231 EVs and BT-474 EVs. Under electron microscopy, BT-474 EVs displayed a characteristic saucer-shaped morphology (Fig. 1d), and Nanosight data displayed that the majority of isolated BT-474 EVs were between 100 and 150 nm in diameter (Fig. 1e) with average size of 122 nm.

We incubated 1×10^{10} BT-474 EVs with 4×10^4 starved MDA-MB-231 cells for 2 h, 6 h, and 12 h, respectively. The EV-cell plasma membrane fusion directly imprinted BT-474 cell-derived HER2 on MDA-MB-231 cell membranes, and thus the educated MDA-MB-231 cells were successfully observed with fluorescence labeled anti-HER2 antibodies (Fig. 1f). Western blot analysis revealed 2-h incubation was insufficient as the amount of HER2 did not show significant change in comparison with the counterpart. At 6 h and 12 h timepoints, the quantified data show that signal intensities of HER2 derived from educated MDA-MB-231 cells were 2.47- and 8.75-fold higher than those of negative controls (Fig. 1g). Therefore, we chose 12-h incubation for further optimization. Of note, in our previous study we demonstrated EVs can be internalized by cells at 2 h timepoint [43]. In fact, when EVs reach the plasma membrane the internalization of EVs only takes ~3 min after the initial interaction [44]. Nevertheless, the extended incubation time can benefit internalization of EVs by recipient cells. Moreover, the Western blot of membrane proteins extracted from educated MDA-MB-231 cells further demonstrated HER2 derived from BT-474 EVs can be integrated to MDA-MB-231 cell membrane (Fig. 1h). Next, $\sim 4 \times 10^4$ MDA-MB-231 cells were educated with $\sim 1 \times 10^9$, $\sim 1 \times 10^8$, and $\sim 1 \times 10^7$ BT-474 EVs for 12 h. The signal intensity of HER2 derived from educated MDA-MB-231 cells decreased along with the decreased amount of BT-474 EVs. The quantified data show that signal intensities of HER2 derived from educated MDA-MB-231 cells in the former two groups were 5.62- and 2.33-fold higher than those of negative controls. No significant difference in HER2 was found in $\sim 1 \times 10^7$ BT-474 EVs educated MDA-MB-231 cells (Fig. 1g), indicating limited EVs were internalized. Subsequently, we estimated the amount of conferred HER2 on educated MDA-MB-231 cells. Given uneducated MDA-MB-231 cells inherently harbor $\sim 4 \times 10^4$ HER2, we speculate additional 3.1×10^5, 1.8×10^5, and 5.9×10^4 HER2 were further conferred from $\sim 1 \times 10^{10}$, $\sim 1 \times 10^9$, and $\sim 1 \times 10^8$ BT-474 EVs to recipient cells after 12-h incubation. These imprinted HER2 can remain on MDA-MB-231 cells for at least 24 h. The measured average diameter of BT-474 cells is 13.1 μm. Assuming HER2 homogeneously distributes on plasma, therefore the individual BT-474 EV may harbor ~350 HER2. Then, we deduced that conferral efficiency of HER2 on MDA-MB-231 cells in three groups was 0.35%, 2.06%, and 6.74%, respectively. The low efficiency might be caused by inefficient interaction between EVs in suspension and cells attached on the flask surface. On the other hand, to maintain the optimal surface area to volume ratio we speculate the recipient cells have to reach a dynamic equilibrium between internalization of foreign EVs and release of self-derived EVs, and this unknown kinetics may limit the internalization of foreign EVs. Therefore, EV internalization kinetics and methods for improving the internalization efficiency deserve further investigation. Moreover, it was reported that cells can form early endosomes, multivesicular endosomes, and then release multivesicular compartments via fusion with the plasma membrane in 3 h. The conferred HER2 could be released into the extracellular environment via MDA-MB-231 cell-derived EVs [45]. Furthermore, the conferred HER2 might be internalized. They are

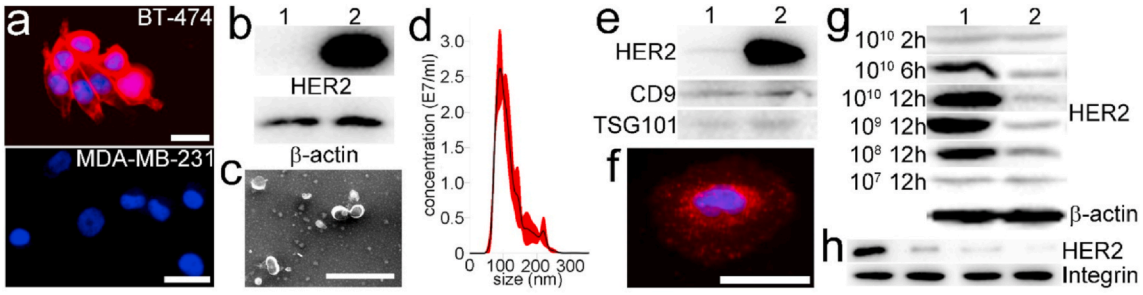

Fig. 1. Characterization of cells and BT-474 EVs. a, fluorescent images of BT-474 and MDA-MB-231 cells. Red: AF594 conjugated anti-HER2 antibody; Blue: DAPI (scale bar, 10 μm). **b**, Western blot of HER2 and β-actin extracted from lysates of MDA-MB-231 cells (1) and BT-474 cells (2). **c**, Morphologic characterization of BT-474 EVs by electron microscopy (scale bar, 500 nm). **d**, Size distribution of BT-474 EVs measured with Nanosight. **e**, Western blot of HER2, CD9, and TSG-101 extracted from lysates of MDA-MB-231 EVs (1) and BT-474 EVs (2). **f**, fluorescent images of BT-474 EV-educated MDA-MB-231 cells at 12 h time point. Red: AF594 conjugated anti-HER2 antibody; Blue: DAPI (scale bar, 10 μm). **g**, Western blot of HER2 and β-actin extracted from lysates of 10^7-10^{10} BT-474 EVs educated MDA-MB-231 cells (1) and untreated MDA-MB-231 cells (2) for 2–12 h **h**, Western blot of HER2 and integrin extracted from plasma membrane of MDA-MB-231 cells educated with 10^{10} BT-474 EVs for 2, 6, and 12 h, respectively. From left to right: 12 h, 6 h, and 2 h education with EVs and negative control. (For interpretation of the references to colour in this figure legend, the reader is referred to the Web version of this article.)

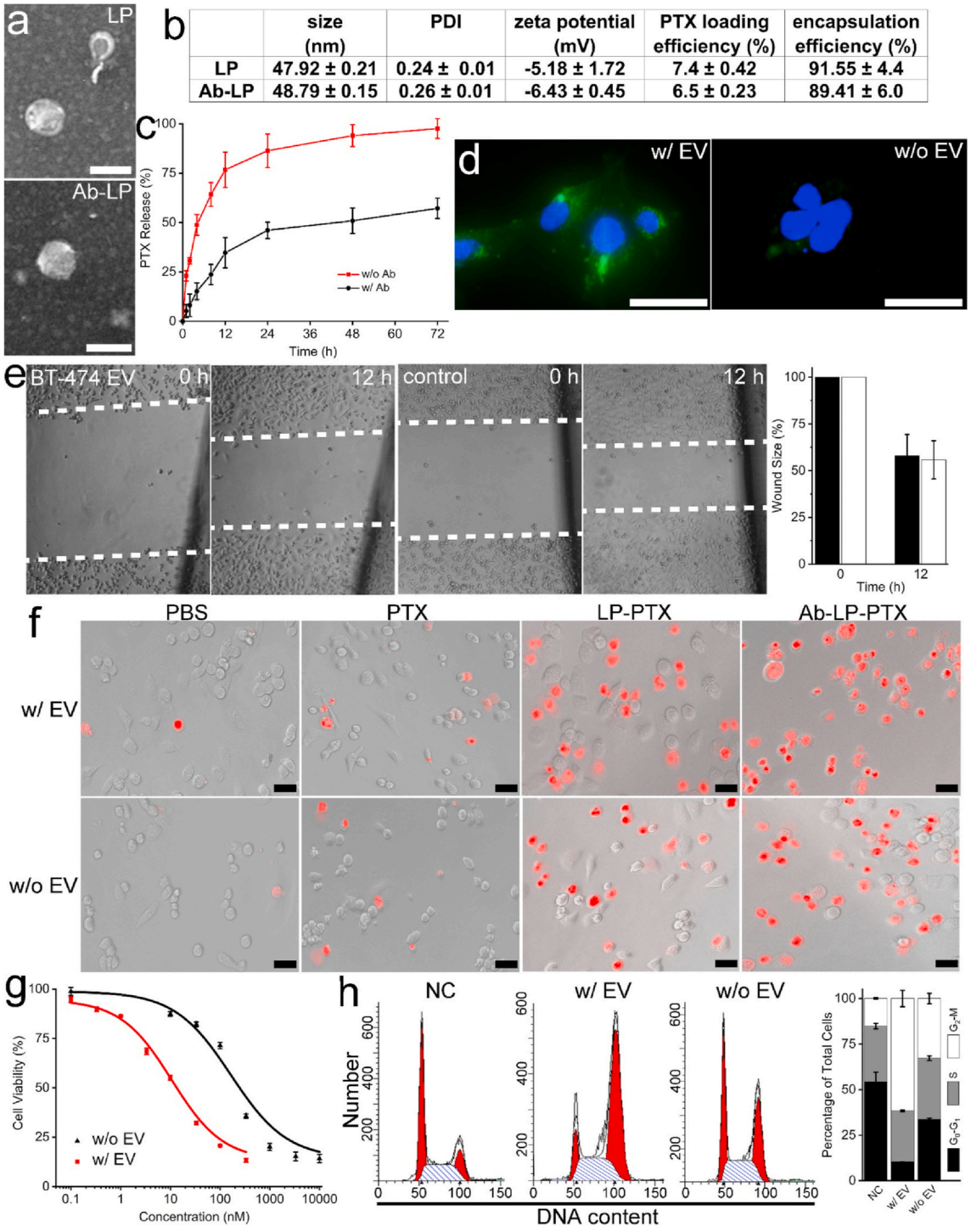

	size (nm)	PDI	zeta potential (mV)	PTX loading efficiency (%)	encapsulation efficiency (%)
LP	47.92 ± 0.21	0.24 ± 0.01	-5.18 ± 1.72	7.4 ± 0.42	91.55 ± 4.4
Ab-LP	48.79 ± 0.15	0.26 ± 0.01	-6.43 ± 0.45	6.5 ± 0.23	89.41 ± 6.0

Fig. 2. Characterization of drug delivery liposome and treatment efficacy. a, Morphologic characterization of LP-PTX and Ab-LP-PTX by electron microscopy (scale bar, 50 nm). **b**, Characterization of LP-PTX and Ab-LP-PTX, including size distribution, PDI, zeta potential, PTX loading efficiency, and PTX release profile. **c**, *In vitro* release of PTX from LP-PTX and Ab-LP-PTX at 37 °C, respectively. **d**, fluorescent images showing Ab-LP binding to HER2-grafted MDA-MB-231 cell surface and to uneducated MDA-MB-231 cell surface at 15 min time point (scale bar, 10 μm). **e**, Wound healing assay of MDA-MB-231 cells educated with BT-474 EVs or uneducated and quantification of wound closure. Migration was assessed at 12 h time point after wounding. **f**, Fluorescence images of HER2-grafted MDA-MB-231 cells and uneducated MDA-MB-231 cells treated with PBS, 100 nmol/L free PTX, LP-PTX, and Ab-LP-PTX, stained with propidium iodide (n = 5). **g**, Respective IC_{50} values of Ab-LP-PTX after 24-h incubation with HER2-grafted MDA-MB-231 cells and uneducated MDA-MB-231 cells, respectively. **h**, Flow cytometry and relevant quantified data of cell cycles of HER2-grafted MDA-MB-231 cells and uneducated MDA-MB-231 cells treated with 100 nmol/L Ab-LP-PTX for 24 h, respectively.

either recycled back to the cell surface after 7–28 h or transported to the late endosome/lysosome for degradation [46]. Nevertheless, to efficiently confer HER2 on MDA-MB-231 cells, we chose 1×10^{10} BT-474 EVs to educate 4×10^{4} cells for 12 h.

Electron microscopy verified that both LPs and Ab-LPs possess a well-defined spherical shape and were homogeneously distributed (Fig. 2a). Slight differences in physical properties were observed between LPs and Ab-LPs due to antibody inclusion (Fig. 2b). The average

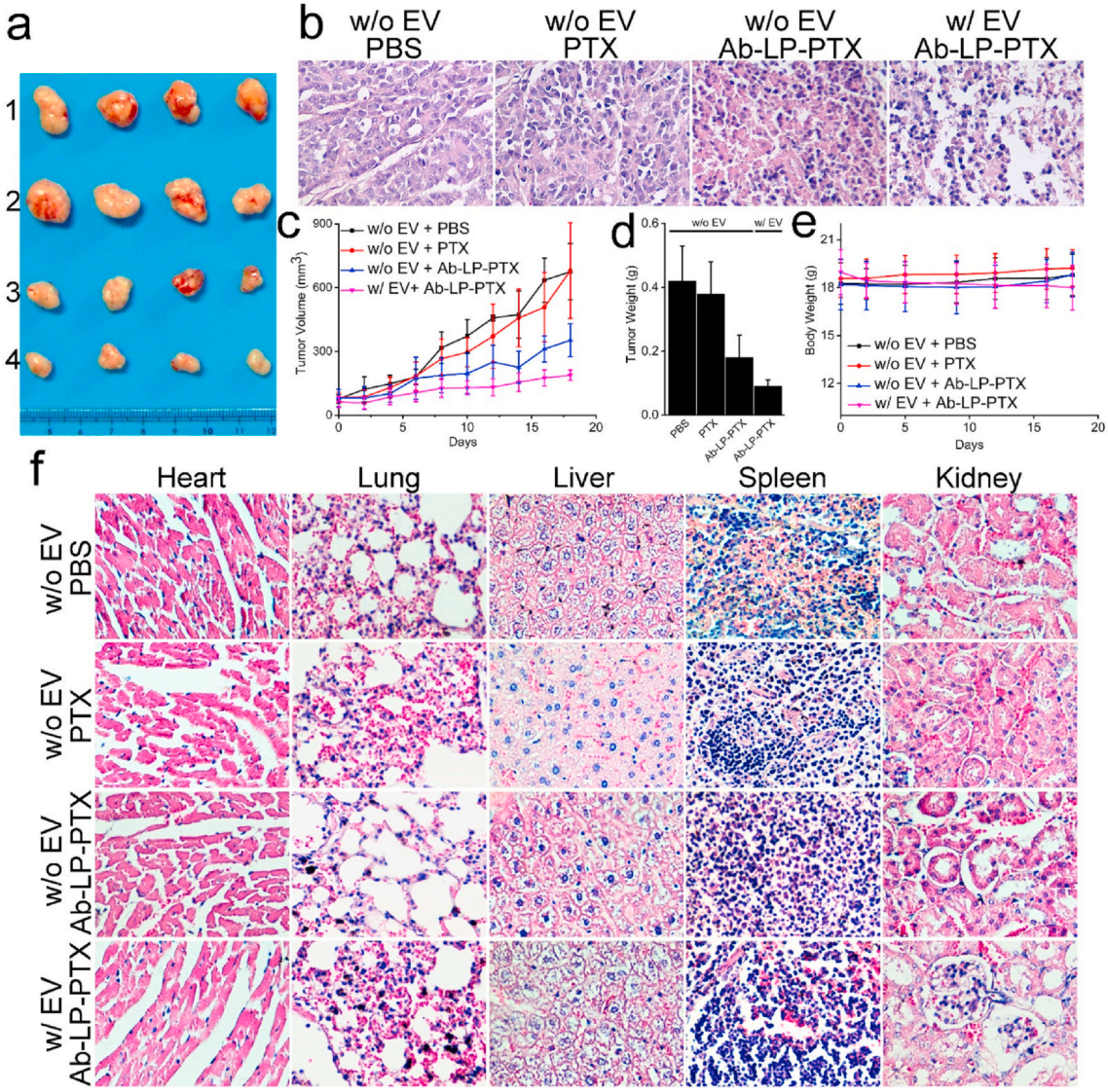

Fig. 3. Tumor treatment *in vivo*. **a**, Tumor tissues obtained from each group of euthanized mice (n = 4) 18 days after administration of w/o EV + PBS (1), w/o EV + free PTX (2), w/o EV + Ab-LP-PTX (3), and w/EV + Ab-LP-PTX (4), respectively. **b**, Typical histologic sections of tumors with HE staining. **c**-**d**, Tumor volume and weight of MDA-MB-231 tumor xenograft in mice from each group after drug or placebo administration (n = 4). **e**, Average mass of mice from each group without significant difference (n = 4). **f**, HE staining of major organs and tumor in each group.

diameters of LPs and Ab-LPs were 47.92 nm and 48.79 nm, respectively. Polydispersity indices (PDIs) were measured as 0.24 ± 0.01 and 0.26 ± 0.01 for LPs and Ab-LPs, respectively. Immobilization of HER2 antibodies on the liposomal membrane decreased the mean zeta potential of the LPs from −5.18 mV to −6.43 mV, ensuring the stability of both during blood circulation. A decrease in PTX loading efficiency from 7.4% to 6.5% was observed in Ab-LPs compared to LPs which was caused by the additional antibody conjugation and rinsing. Regardless of antibody inclusion, PTX encapsulation efficiency was similar, around 90%. We further investigated the release kinetics of LP-PTX and Ab-LP-PTX at 37 °C, respectively. Both exhibited burst release kinetics over the first 6 h followed by an extended sustained release profile over the next 64 h (Fig. 2c). At the 24-h time point, LP-PTX and Ab-LP-PTX had released approximately 85% and 45% PTX, respectively. The slower release rate demonstrated by the Ab-LP-PTX suggests a significantly superior *in vitro* administration profile. The loaded PTX can therefore be safely delivered to cells, avoiding early release and partially ameliorating off-target effects. Next, the BT-474 EV-educated MDA-MB-231 cells and uneducated MDA-MB-231 cells were incubated with Ab-LPs. Fluorescence confirmed Ab-LPs could quickly recognize the incorporated HER2 and significantly bind to MDA-MB-231 cells within just 15 min (Fig. 2d). In contrast, fluorescence signal was undetectable in control group at the same time point, indicating very few Ab-LPs attached and fused with uneducated MDA-MB-231 cell membranes. Altogether, successful integration of ~9-fold more HER2 into MDA-MB-231 cell membranes should hereby allow for subsequent HER2 targeted drug delivery.

Treatment of cancer cells *in vitro* and *in vivo*. As noted, both cell types have previously exhibited the ability to transfer oncogenic payloads, consisting of proteins and RNAs responsible for a myriad of pro-tumor characteristics, to somatic cells [47,48]. The ability of highly aggressive MDA-MB-231 and BT-474 cells to imprint more metastatic phenotypes onto less aggressive cells, including healthy cells, is highly documented [49]. However, whether BT-474 EVs can reduce the metastatic potential of MDA-MB-231 cells is unclear. In order to confirm that no ancillary education effect of BT-474 EVs was responsible for treatment efficacy, a wound healing assay was performed as a simple proxy for metastatic potential. No discernible difference was found between the wound closure rates of EV-educated MDA-MB-231 cells compared to their uneducated counterparts (Fig. 2e). After 12 h, both

wound widths were ~60% and had closed before the 24 h time point. Given education with BT-474 EVs did result in the integration of HER2 into MDA-MB-231 membranes, as evidenced by anti-HER2 fluorescence staining (Fig. 1e), in the reduction metastatic potential of MDA-MB-231 cells via education with BT-474 EVs is seemingly non-existent. In the following experiments, the enhanced treatment effects were therefore assumed to be a product of the integrated HER2 and targeted drug delivery.

A marked difference in treatment efficacy, as observed by PI staining, was found between Ab-LP-PTX group and the other groups, with the former inducing apoptosis of almost all MDA-MB-231 cells (Fig. 2f). In group of EV-educated MDA-MB-231, average 1.76%, 15.2%, 40.3%, and 97.8% cells treated with PBS, free PTX, LP-PTX, and Ab-LP-PTX show detectable red fluorescence signal. In control group of uneducated MDA-MB-231 cells, 2.94%, 12.2%, 38.8%, and 61.1% cells showed red fluorescence signal in each subgroup. Significant difference in amount of apoptotic cells was found between Ab-LP-PTX treated EV-educated and uneducated MDA-MB-231 cells (*t*-test, $p < 0.01$), demonstrating the conferred HER2 could promote the treatment efficacy of targeted drug delivery. Subsequently, we directly used Ab-LP-PTX to treat EV-educated and uneducated MDA-MB-231 cells. The IC_{50} of Ab-LP-PTX in two groups was 9.9 nM and 173 nM, respectively (*t*-test, $p < 0.01$). Therefore, with equal amount of Ab-LP-PTX the treatment efficacy of EV-educated MDA-MB-231 cells can be significantly improved by 17.5-fold. Alternatively, to reach the equivalent treatment efficacy, the EV-educated MDA-MB-231 cells would require significantly less PTX in comparison with that of counterpart (Fig. 2g). Moreover, flow cytometry data indicated the treatment of Ab-LP-PTX caused ~65% EV-educated cells to retain in the G_2-M phase. In contrast, ~30% of uneducated cells retain in this phase after the same treatment, underlining Ab-LP-PTX can more efficiently prevent mitosis of HER2 conferred cells compared to that of uneducated cells (Fig. 2h).

Next, we investigated the efficacy of anti-HER2 drug delivery in xenograft BALB/c mouse models. A therapeutically ineffective dosing of free PTX, 2 mg of PTX-equivalent per kg of body weight per dose, was specifically chosen in order to highlight the potential differences in treatment. In the first two negative control groups, PBS and free PTX was used to treat uneducated tumor. The free PTX did not inhibit tumor growth as designed (Fig. 3a). In the latter two groups, Ab-LP-PTX was used to treat uneducated MDA-MB-231 cells and BT-474 EV educated MDA-MB-231 cells. Following tumor harvesting, Ab-LP-PTX treated mice displayed significantly reduced average tumor weights and volumes (Fig. 3a). Moreover, in the fourth group, the tumor educated with BT-474 EVs showed the smaller volume and that of tumor without EV education. Histological analysis of tumor tissue revealed enhanced destructive capabilities of the Ab-LP-PTX over those of PBS and free PTX (Fig. 3b). Similarly, Ab-LP-PTX treated EV-educated tumor demonstrated significant destruction of the tumor tissue. It indicates that even a normally ineffective PTX dose is still successful in inhibiting tumor growth when used to target inserted HER2. Harvested tumors from four groups were found to have average volumes of 675, 680, 352, and 188 mm^3, respectively and weight of 0.42, 0.38.0.18, and 0.10 g, respectively (ANOVA, $p < 0.05$) (Fig. 3c–d). The use of targeted delivery to treat educated tumors therefore decreased the average tumor weight by 34.6% and the average volume by 33.3% over 18 days. No significant cachexia was observed in any of the subjects. There was no significant difference in mouse body weight during the administration either (Fig. 3e). Tissue samples were further taken from the heart, lungs, spleen, and kidney of each subject for histological analysis. Extensive damage in major organs was not observed in any groups (Fig. 3f). However, slight difference in HE staining may indicate a favorable lack of tissue damage for the Ab-LP-PTX treatment of EV educated tumor compared to the others. Thus, compared to free PTX and Ab-LP-PTX in treatment of uneducated tumor, higher dose of Ab-LP-PTX can be administrated to kill HER2 conferred tumor, improving the chemotherapeutic effects without the occurrence of severe adverse reactions.

4. Discussion

The quest to obtain an effective treatment for TNBC has hitherto been met with considerable frustration. The most insurmountable portion of this triple negative problem is the distinct lack of targetable receptors, most notable HER2, which prevents TNBC from being swept into the burgeoning wave of immunotherapeutic treatments [50]. While ongoing clinical trials are investigating the safety and efficacy of PD-1, PD-L1, and CTLA-4 inhibitors in TNBC, chemotherapy largely of completely unrelated cells has been, and continues to be, extensively elucidated. As has been elegantly reported, EVs carrying membrane proteins representative of their parent cells have demonstrated the ability to confer these proteins on the recipient cell's membrane via membrane fusion [51–53]. Hence, this paper represents a new approach to converting tumor phenotype by imposing targetable receptors into the membrane of deficient cells via EV membrane fusion. We demonstrated that the use of targeted therapy in conjunction with this receptor grafting is superior to the use of therapies without receptor grafting. Not only was membrane insertion and targeted delivery more effective in decreasing tumor size, it showed advantageous qualities in terms of IC_{50} and reduced off-target effects. This proof-of-concept showed promise in both *in vitro* and *in vivo* models.

It is noteworthy that the conferral of antigens via membrane fusion and intratumoral injection is transient (~24 h), thus minimizing potential tumorigenicity, as HER2 overexpression is associated with a myriad of tumorigenic activities [54]. The vast majority of TNBC cells lack the capacity to self-reproduce HER2 once the infusion of $HER2^+$ EVs stops. Cells that do not natively express HER2 will undo its integration via dynamic remodeling of the cell membrane or lose the conferred HER2 once it is transported to the late endosome/lysosome for degradation or release to extracellular space. The simple insertion of desirable membrane receptors is thus a double-edged sword. Overexpression and dysregulation in healthy cells is largely avoided, but treatment efficacy is dependent on the continuing infusion of EVs. It is worthwhile to note that intratumoral injection is very flexible in terms of conferring various targetable antigens, such as programmed death-ligand 1 (PD-L1), prostate-specific antigen (PSA), and carbonic anhydrase IX (CA IX) on receipt cell membrane for targeted therapy. What antigens can be inserted is limited only to the existence of harvestable EVs that possess that receptor. In future work, BT-474 EV cargo, with the exception of HER2, can be entirely depleted to limit undesired effects and specific EV subpopulations that are more prone to membrane fusion could be selected to fine tune the efficiency of conferral.

On the other hand, intratumoral injection of $HER2^+$ EVs for inoculation of TNBC cells before intravenous administration of drugs may impractical in cancer patients, and thus further development of this prototyping approach may be desired. For instance, the homing of mRNA- and/or retrotransposon element-encapsulated EVs to the solid tumor could be an alternative and feasible approach. Such a method would initiate the synthesis, and subsequent membrane integration, of targetable HER2 onto the plasma membrane of recipient cells. Similarly, favorable mRNAs could be used to stimulate the expression of a wide variety of antigens, such as PD-L1, so as to convert tumors into phenotypes favorable for existing chemo- or immunotherapies. While the overexpression of these receptors has been linked to enhanced proliferation, motility, and invasion of cancer cells [54], the now immunologically revised hot tumors would contain more surface antigens and higher levels of infiltrating T cells. As a result, these cells would be more recognizable to the host's immune system, thus increasing the likelihood of triggering a strong immune response. Consequently, cancer patients may derive greater benefit from conventional targeted drug delivery and/or immunotherapy such as CAR-T and monoclonal antibody therapy. Nevertheless, delivery of mRNA and/or retrotransposon elements may permanently alter the phenotype of recipient

cells, and hence may promote tumorigenicity to a certain extent.

Altogether, this proof-of-concept represents a unique method of priming tumor cells for targeted delivery or immunotherapy via the conferral of relevant receptors. The ease of implementation, favorable intrinsic characteristics of EVs, and reliance on previously tested drug delivery systems make this potential treatment conducive to extensive alteration and possible clinical translation.

CRediT authorship contribution statement

Zachary Quinn: Conceptualization, Methodology, Software, Validation, Formal analysis, Investigation, Data curation, Writing - review & editing. **Wenjun Mao:** Conceptualization, Methodology, Validation, Formal analysis, Investigation, Resources, Data curation, Writing - review & editing, Supervision. **Yiqiu Xia:** Validation. **Rhea John:** Software, Validation, Visualization. **Yuan Wan:** Conceptualization, Formal analysis, Resources, Writing - review & editing, Supervision, Project administration, Funding acquisition.

Declaration of competing interest

All authors declare that they have no conflicts of interest and no competing interest.

Acknowledgements

This work was partially supported by Binghamton University Faculty Startup Fund 910252-35 and Binghamton University S3IP award ADLG195.

References

[1] L.A. Torre, R.L. Siegel, E.M. Ward, A.J.C.E. Jemal, P. Biomarkers, Global Cancer Incidence and Mortality Rates and Trends—An Update vol. 25, (2016), pp. 16–27.
[2] V.S. Jamdade, N. Sethi, N.A. Mundhe, P. Kumar, M. Lahkar, N. Sinha, Therapeutic targets of triple-negative breast cancer: Rev. 172 (2015) 4228–4237.
[3] F. Penault-Llorca, G.J.A.o.o. Viale, Pathological and Molecular Diagnosis of Triple-Negative Breast Cancer: a Clinical Perspective vol. 23, (2012), pp. vi19–vi22.
[4] B.D. Lehmann, J.A. Bauer, X. Chen, M.E. Sanders, A.B. Chakravarthy, Y. Shyr, J.A. Pietenpol, Identification of Human Triple-Negative Breast Cancer Subtypes and Preclinical Models for Selection of Targeted Therapies vol. 121, (2011), pp. 2750–2767.
[5] Rebecca Dent, Maureen Trudeau, Kathleen I. Pritchard, Wedad M. Hanna, HarrietK. Kahn, Carol A. Sawka, Lavina A Lickley, Ellen Rawlinson, Ping Sun, Steven A Narod, Triple-negative breast cancer: clinical features and patterns of recurrence 13 (2007) 4429–4434.
[6] N.U. Lin, E. Claus, J. Sohl, A.R. Razzak, A. Arnaout, E.P.J.C. Winer, Sites of Distant Recurrence and Clinical Outcomes in Patients with Metastatic Triple-negative Breast Cancer: High Incidence of Central Nervous System Metastases vol. 113, (2008), pp. 2638–2645.
[7] H. Sihto, J. Lundin, M. Lundin, T. Lehtimäki, A. Ristimäki, K. Holli, L. Sailas, V. Kataja, T. Turpeenniemi-Hujanen, J.J.B.C.R. Isola, Breast cancer biological subtypes and protein expression predict for the preferential distant metastasis sites, a nationwide cohort study 13 (2011) R87.
[8] Lisa A Carey 1, E Claire Dees, Lynda Sawyer, Lisa Gatti, Dominic T Moore, Frances Collichio, David W Ollila, Carolyn I Sartor, Mark L Graham, Charles M Perou, The triple negative paradox: primary tumor chemosensitivity of breast cancer subtypes, 13 (2007) 2329–2334.
[9] N.U. Lin, A. Vanderplas, M.E. Hughes, R.L. Theriault, S.B. Edge, Y.N. Wong, D.W. Blayney, J.C. Niland, E.P. Winer, J.C.J.C. Weeks, Clinicopathologic features, patterns of recurrence, and survival among women with triple-negative breast cancer in the, National Comprehensive Cancer Network 118 (2012) 5463–5472.
[10] S.B. Zeichner, H. Terawaki, K.J.B.c.b. Gogineni, c. research, A Review of Systemic Treatment in Metastatic Triple-Negative Breast Cancer vol. 10, BCBCR, 2016, p. S32783.
[11] P. Sharma, S. Hu-Lieskovan, J. Wargo, A.J.C. Ribas, Leading edge review primary, adaptive, and acquired resistance to cancer, Immunotherapy 168 (2017) 707–723.
[12] Drew M. Pardoll, The Blockade of Immune Checkpoints in Cancer Immunotherapy vol. 12, (2012), pp. 252–264.
[13] Russell W Jenkins, David A. Barbie, Keith T Flaherty, Mechanisms of resistance to immune checkpoint inhibitors, 118 (2018) 9–16.
[14] Leisha A Emens, Breast cancer immunotherapy: facts and hopes 24 (2018) 511–520.
[15] P. Bonaventura, T. Shekarian, V. Alcazer, J. Valladeau-Guilemond, S. Valsesia-Wittmann, S. Amigorena, C. Caux, S.J.F.i.i. Depil, Cold tumors: a therapeutic challenge for immunotherapy 10 (2019) 168.
[16] L.J.F.i.O. Sevenich, Turning "Cold" into "Hot" Tumors—Opportunities and Challenges for Radio-Immunotherapy against Primary and Metastatic Brain Cancers vol. 9, (2019), p. 163.
[17] P. Srivastava, B.E. Paluch, J. Matsuzaki, S.R. James, G. Collamat-Lai, J. Karbach, M.J. Nemeth, P. Taverna, A.R. Karpf, E.A.J.L.r. Griffiths, Immunomodulatory action of SGI-110, a hypomethylating agent, acute myeloid leukemia cells and xenografts 38 (2014) 1332–1341.
[18] J. Dunn, S.J.M.i. Rao, Epigenetics and immunotherapy: the current state of play 87 (2017) 227–239.
[19] E. Willms, C. Cabañas, I. Mäger, M.J. Wood, P.J.F.i.i. Vader, Extracellular vesicle heterogeneity: subpopulations, isolation techniques, and diverse functions in cancer progression 9 (2018) 738.
[20] Y. Fujita, Y. Yoshioka, T.J.C.s. Ochiya, Extracellular vesicle transfer of cancer pathogenic components 107 (2016) 385–390.
[21] Liliana Czernek, Markus Duechler, Functions of cancer-derived extracellular vesicles in immunosuppression 65 (2017) 311–323.
[22] A. Becker, B.K. Thakur, J.M. Weiss, H.S. Kim, H. Peinado, D.J.C.c. Lyden, Extracellular vesicles in cancer: cell-to-cell mediators of metastasis 30 (2016) 836–848.
[23] T.B. Steinbichler, J. Dudás, H. Riechelmann, I.-I. Skvortsova, The role of exosomes in cancer metastasis, Seminars in Cancer Biology, Elsevier, 2017, pp. 170–181.
[24] G. Chen, A.C. Huang, W. Zhang, G. Zhang, M. Wu, W. Xu, Z. Yu, J. Yang, B. Wang, H.J.N. Sun, Exosomal PD-L1 Contributes to Immunosuppression and Is Associated with Anti-PD-1 Response vol. 560, (2018), pp. 382–386.
[25] J.P. Webber, L.K. Spary, A.J. Sanders, R. Chowdhury, W.G. Jiang, R. Steadman, J. Wymant, A.T. Jones, H. Kynaston, M.D.J.O. Mason, Differentiation of tumour-promoting stromal myofibroblasts by cancer exosomes 34 (2015) 290–302.
[26] N. Tominaga, N. Kosaka, M. Ono, T. Katsuda, Y. Yoshioka, K. Tamura, J. Lötvall, H. Nakagama, T.J.N.c. Ochiya, Brain Metastatic Cancer Cells Release microRNA-181c-Containing Extracellular Vesicles Capable of Destructing Blood–Brain Barrier vol. 6, (2015), pp. 1–12.
[27] Marc A. Antonyak, Bo Li, Lindsey K. Boroughs, Jared L. Johnson, Joseph E. Druso, Kirsten L. Bryant, David A. Holowka, Richard A. Cerione, Cancer Cell-Derived Microvesicles Induce Transformation by Transferring Tissue Transglutaminase and Fibronectin to Recipient Cells vol. 108, (2011), pp. 4852–4857.
[28] A. Zomer, C. Maynard, F.J. Verweij, A. Kamermans, R. Schäfer, E. Beerling, R.M. Schiffelers, E. de Wit, J. Berenguer, S.I.J.J.C. Ellenbroek, In Vivo Imaging Reveals Extracellular Vesicle-Mediated Phenocopying of Metastatic Behavior vol. 161, (2015), pp. 1046–1057.
[29] J. Che, C. I Okeke, Z.-B. Hu, J.J.C.p.d. Xu, DSPE-PEG: a distinctive component in drug delivery system 21 (2015) 1598–1605.
[30] Susan M van Dommelen, P. Vader, Samira Lakhal, S A A Kooijmans, Wouter W van Solinge, Matthew J A Wood, Raymond M Schiffelers, Microvesicles and Exosomes: Opportunities for Cell-Derived Membrane Vesicles in Drug Delivery vol. 161, (2012), pp. 635–644.
[31] S.-i. Ohno, M. Takanashi, K. Sudo, S. Ueda, A. Ishikawa, N. Matsuyama, K. Fujita, T. Mizutani, T. Ohgi, T.J.M.T. Ochiya, Systemically Injected Exosomes Targeted to EGFR Deliver Antitumor microRNA to Breast Cancer Cells vol. 21, (2013), pp. 185–191.
[32] Jasper G van den Boorn, Juliane Dassler, Christoph Coch, Martin Schlee, Gunther Hartmann, Exosomes as nucleic acid nanocarriers 65 (2013) 331–335.
[33] O.Y. Kim, J. Lee, Y.S. Gho, Extracellular vesicle mimetics: novel alternatives to extracellular vesicle-based theranostics, drug delivery, and vaccines, Seminars in Cell & Developmental Biology, Elsevier, 2017, pp. 74–82.
[34] Isabella Parolini, Cristina Federici, Carla Raggi, Luana Lugini, Simonetta Palleschi, Angelo De Milito, Carolina Coscia, Elisabetta Iessi, Mariantonia Logozzi, Agnese Molinari, Marisa Colone, Massimo Sargiacomo, Stefano Fais, Microenvironmental pH is a key factor for exosome traffic in tumor cells, 284 (2009) 34211–34222.
[35] Masamitsu Kanada, Michael H Bachmann, Jonathan W Hardy, Daniel Omar Frimannson, Laura Bronsart, Andrew Wang, Matthew D Sylvester, Tobi L Schmidt, Roger L Kaspar, Manish J Butte, A C Matin Butte, Christopher H Contag, Differential fates of biomolecules delivered to target cells via extracellular vesicles, 112 (2015) E1433–E1442.
[36] R. Jahn, T. Lang, T.C.J.C. Südhof, Membrane fusion 112 (2003) 519–533.
[37] L.V. Chernomordik, M.M.J.N.s. Kozlov, m. biology, Mechanics of membrane fusion 15 (2008) 675–683.
[38] S.M. Park, M.S. Kim, S.J. Park, E.S. Park, K.S. Choi, Y.s. Kim, H.R. Kim, Novel temperature-triggered liposome with high stability: formulation, in vitro evaluation, and in vivo study combined with high-intensity focused ultrasound, HIFU) 170 (2013) 373–379.
[39] Danny L. Costantini, Katherine. Bateman, Kristin McLarty, Katherine A. Vallis, Raymond M. Reilly, Trastuzumab-resistant breast cancer cells remain sensitive to the auger electron–emitting radiotherapeutic agent 111In, NLS-trastuzumab and are radiosensitized by methotrexate 49 (2008) 1498–1505.
[40] Bart S. Hendriks, Stephan G. Klinz, Joseph G. Reynolds, Christopher W. Espelin, Daniel F. Gaddy, Thomas J. Wickham, Impact of tumor HER2/ERBB2 expression level on HER2-targeted liposomal doxorubicin-mediated drug delivery: multiple low-affinity interactions lead to a threshold effect, 12 (2013) 1816–1828.
[41] Helen J Hathaway, Kimberly S Butler, Natalie L Adolphi, Debbie M Lovato, Robert Belfon, Danielle Fegan, Todd C Monson, Jason E Trujillo, Trace E Tessier, Howard C Bryant, Dale L Huber, Richard S Larson, Edward R Flynn, Detection of breast cancer cells using targeted magnetic nanoparticles and ultra-sensitive magnetic field, Sensors 13 (2011) R108.
[42] Adrian V. Lee, Steffi Oesterreich, Nancy E. Davidson, MCF-7 Cells—Changing the Course of Breast Cancer Research and Care for 45 Years, (2015), p. 107.

[43] Yuan Wan, Gong Cheng, Xin Liu, Si-Jie Hao, Merisa Nisic, Chuan-Dong Zhu, Yi-Qiu Xia, Wen-Qing Li, Zhi-Gang Wang, Wen-Long Zhang, Shawn J. Rice, Aswathy Sebastian, Istvan Albert, Chandra P. Belani, Si-Yang Zheng, Rapid magnetic isolation of extracellular vesicles via lipid-based nanoprobes 1 (2017) 1–11.
[44] Tian Tian, Yan-Liang Zhu, Fei-Hu Hu, Yuan-Yuan Wang, Ning-Ping Huang, Zhong-Dang Xiao, Dynamics of exosome internalization and trafficking 228 (2013) 1487–1495.
[45] C. Théry, L. Zitvogel, S.J.N.r.i. Amigorena, Exosomes: composition, biogenesis and function 2 (2002) 569–579.
[46] O. Shilova, G. Proshkina, E. Lebedenko, S.J.A.N. Deyev, Internalization and Recycling of the HER2 Receptor on Human Breast Adenocarcinoma Cells Treated with Targeted Phototoxic Protein DARPinminiSOG vol. 7, (2015).
[47] S. Kruger, Z.Y. Abd Elmageed, D.H. Hawke, P.M. Wörner, D.A. Jansen, A.B. Abdel-Mageed, E.U. Alt, R.J.B.c. Izadpanah, Molecular Characterization of Exosome-like Vesicles from Breast Cancer Cells vol. 14, (2014), pp. 1–10.
[48] G. Palazzolo, N.N. Albanese, G. Di Cara, D. Gygax, M.L. Vittorelli, I.J.A.r. Pucci-Minafra, Proteomic Analysis of Exosome-like Vesicles Derived from Breast Cancer Cells vol. 32, (2012), pp. 847–860.
[49] J. Peng, W. Wang, S. Hua, L.J.B.c.b. Liu, c. research, Roles of Extracellular Vesicles in Metastatic Breast Cancer vol. 12, (2018) 1178223418767666.
[50] H. Katz, M.J.M.O. Alsharedi, Immunotherapy in Triple-Negative Breast Cancer vol. 35, (2018), p. 13.
[51] L. Mulcahy, R. Pink, D. Carter, Routes and mechanisms of extracellular vesicle uptake, J. Extracell. Vesicles 3 (2014) 24641.
[52] M. Mathieu, L. Martin-Jaular, G. Lavieu, C.J.N.c.b. Thery, Specificities of Secretion and Uptake of Exosomes and Other Extracellular Vesicles for Cell-To-Cell Communication vol. 21, (2019), pp. 9–17.
[53] Ilaria Prada, Jacopo Meldolesi, Binding and Fusion of Extracellular Vesicles to the Plasma Membrane of Their Cell Targets vol. 17, (2016), p. 1296.
[54] Xing-Hua Liao, Da-Lin Lu, Nan Wang, Long-Yue Liu, Yue Wang, Yan-Qi Li, Ting-Bao Yan, Xue-Guang Sun, Peng Hu, Tong-Cun Zhang, Estrogen Receptor α Mediates Proliferation of Breast Cancer MCF–7 Cells via a p21/PCNA/E 2 F 1-dependent Pathway vol. 281, (2014), pp. 927–942.